

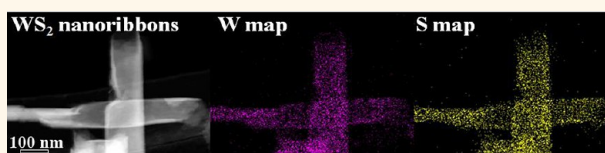
Chemical Unzipping of WS₂ Nanotubes

C. Nethravathi,^{†,*} A. Anto Jeffery,[‡] Michael Rajamathi,^{‡,*} Naoyuki Kawamoto,[†] Reshef Tenne,[#] Dmitri Golberg,^{†,*} and Yoshio Bando[†]

[†]World Premier International (WPI) Center for Materials Nanoarchitectonics (MANA), National Institute for Materials Science (NIMS), Namiki 1-1, Tsukuba, Ibaraki 305-0044, Japan, [‡]Materials Research Group, Department of Chemistry, St. Joseph's College, 36 Lalbagh Road, Bangalore 560 027, India, and

[#]Department of Materials and Interfaces, Weizmann Institute, Rehovot 76100, Israel

ABSTRACT WS₂ nanoribbons have been synthesized by chemical unzipping of WS₂ nanotubes. Lithium atoms are intercalated in WS₂ nanotubes by a solvothermal reaction with *n*-butyllithium in hexane. The lithiated WS₂ nanotubes are then reacted with various solvents—water, ethanol, and long chain thiols. While the tubes break into pieces when treated with water and ethanol, they unzip through longitudinal cutting along the axes to yield nanoribbons when treated with long chain thiols, 1-octanethiol and 1-dodecanethiol. The slow diffusion of the long chain thiols reduces the aggression of the reaction, leading to controlled opening of the tubes.



KEYWORDS: WS₂ nanotubes · unzipping · WS₂ nanoribbons · octanethiol

One-dimensional (1D) nanoribbons of layered solids have gained a lot of interest from both theoretical and experimental points of view because they exhibit unique and distinct properties compared to their two-dimensional (2D) counterparts.^{1,2} In contrast to semimetallic 2D graphene, graphene ribbons of sub-10 nm width are semiconductors whose band gap is inversely dependent on the ribbon width.^{3,4} Similarly, boron nitride nanoribbons are semiconducting, while the 2D boron nitride layers are insulating.^{5,6}

Layers of transition metal dichalcogenides (TMDs) such as MoS₂ and WS₂ are archetypical examples of inorganic analogues of graphene.^{7–9} In contrast to the monoatom thick graphene, the layer of a TMD is three atoms thick with the composition MX₂ where M = Mo, W, Ta, Ti, Nb and X = S, Se, Te. In TMDs, each hexagonal layer of metal atoms (M) is sandwiched between two layers of chalcogen atoms (X). While the atoms within these trilayer sheets are bonded covalently, the weak bonding between adjacent sheets is due to van der Waals interactions.^{7–9} Theoretical calculations reveal that the MoS₂ nanoribbons are magnetic semiconductors (armchair edges) or metallic (zigzag edges),^{10–12} while the ultranarrow WS₂ nanoribbons remain nonmagnetic semiconductors with narrow gap in the case of armchair edges or are metallic (magnetic or nonmagnetic) when

they have zigzag edges in contrast to nonmagnetic and semiconducting bulk WS₂.¹³ Recently, there have been reports on the synthesis of ultranarrow MoS₂/WS₂ nanoribbons inside carbon nanotubes^{11,13} and the synthesis of microribbons of WS₂.¹⁴ However, so far, there has been no report on the synthesis of free-standing WS₂ nanoribbons.

Though graphene nanoribbons could be achieved through chemical synthesis^{15,16} (bottom-up approach), unzipping of carbon nanotubes by various methods has been a promising and efficient approach as these routes are facile and result in high yield.^{1,2} More importantly, opening of carbon nanotubes of <100 nm in diameter and fewer multiwalls can result in ribbons of mono- or few layers with widths of only a few nanometers. Nanotubes could be unzipped by plasma etching,^{17,18} chemical oxidation,^{19,20} intercalation and exfoliation,^{21–23} metal-catalyzed cutting,^{24,25} electrochemical²⁶ or sonochemical means,^{27,28} and laser-induced unzipping.²⁹ Intercalation of alkali metal in the nanotubes followed by violent exfoliation in ethanol has been shown to result in high yield of pristine nonfunctionalized ribbons of graphene^{21,22} or boron nitride.²³ TMDs are also known to form nanotubes.^{30–32} Therefore, it should be possible to form nanoribbons of TMDs by unzipping the TMD nanotubes.

While synthesis of nanoribbons of TMDs, such as WS₂, is an important task, a far more

* Address correspondence to nethravathic@gmail.com, mikerajamathi@rediffmail.com, golberg.dmitri@nims.go.jp.

Received for review June 12, 2013 and accepted July 20, 2013.

Published online July 20, 2013 10.1021/nn4029635

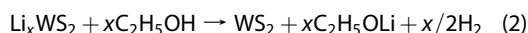
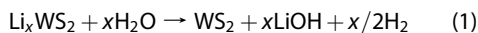
© 2013 American Chemical Society

important challenge is the unzipping of the highly reactive and easy-to-oxidize WS₂ nanotubes that would establish the universal applicability of nanotube unzipping in nanoribbon synthesis. In this article, we demonstrate unzipping of multiwalled WS₂ nanotubes through intercalation followed by exfoliation. The detailed theoretical verification of the process will separately be presented elsewhere.

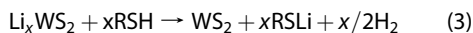
RESULTS AND DISCUSSION

Figure 1a is a bright-field TEM image of the as-received pristine WS₂ nanotubes (WS₂-NTs). The tubes are tens of micrometers in length and 20–80 nm in diameter. The HRTEM image (Figure 1b) of an individual WS₂ nanotube (~40 nm in diameter) displays many layers, and the insets show the closed and open ends of nanotubes.

Lithiated WS₂-NTs (Li_xWS₂-NTs) react violently with water^{33,34} and ethanol, liberating H₂ gas, as indicated by the following chemical equations:



While the WS₂-NTs are nearly fully destroyed, giving rise to porous 1D structures decorated with broken pieces of debris, in the case of water (Figure 1c), they are less destroyed in the case of ethanol where a few scroll-like WS₂ are observed due to partial unzipping of nanotubes along with their breaking into pieces (Figure 1d). Ethanol (pK_a = 15.9), being slightly less acidic than water (pK_a = 14), and, more importantly, poorly diffusing due to its larger molecular size, seems to cause less destruction to the nanotubes. This suggests that diffusivity of the solvent molecules seems to control the unzipping of the WS₂-NTs. Therefore, we wanted to explore the process of unzipping of the Li_xWS₂-NTs with larger solvent molecules. Due to the high possibility of oxidation of WS₂, oxygen-containing solvents are not ideal for the unzipping reaction. Hence we chose thiols, such as octanethiol (pK_a = 10.6) and dodecanethiol (pK_a = 10.5–11), to further investigate the role of diffusivity of solvent molecules in the process of unzipping of Li_xWS₂-NTs. Though the thiols are more acidic than water, their lower diffusivity would reduce the rate of the reaction. The thiols would react with Li_xWS₂ according to the chemical equation



The low- and high-magnification SEM images of the WS₂ nanoribbons (WS₂-NRs) obtained by reacting Li_xWS₂-NTs with octanethiol are shown in Supporting Information, Figure S1b,c. WS₂-NRs appear wider, thinner, and more transparent compared to thick nontransparent WS₂-NTs (Figure S1a), suggesting that the Li_xWS₂-NTs are largely unzipped through longitudinal cutting while retaining the 1D morphology and the

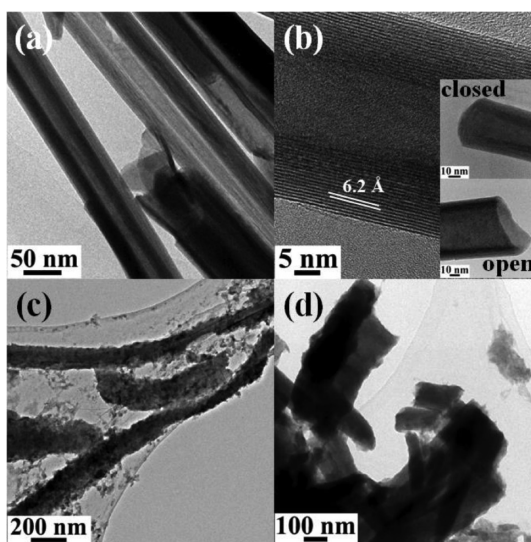


Figure 1. Bright-field TEM (a) and HRTEM (b) images of pristine WS₂-NTs and TEM images of the products obtained when Li_xWS₂-NTs are reacted with water (c) and ethanol (d).

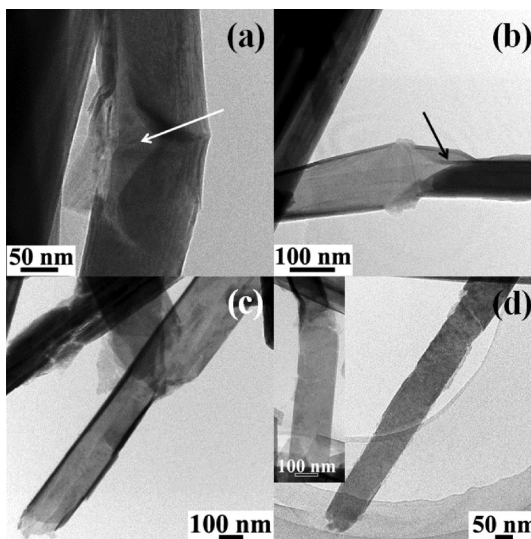


Figure 2. (a–d) Bright-field TEM images of WS₂-NRs obtained by unzipping Li_xWS₂-NTs using octanethiol. The arrows in (a) and (b) mark the incubation stages of the unzipping process.

original length. The XRD pattern (Figure S1d) of the WS₂-NRs was indexed to hexagonal WS₂ (JCPDF no. 87-2417). No peaks due to impurities were observed. Similar results were observed in the case of unzipping of Li_xWS₂-NTs using dodecanethiol. For the sake of brevity, we present the results of WS₂-NRs obtained by reacting Li_xWS₂-NTs with octanethiol only.

The bright-field TEM images of WS₂-NRs are shown in Figure 2. Figure 2a,b reveals details of the processes—initial burst (Figure 2a) and subsequent progress of the incision along the length of the tube (Figure 2b)—involved in splitting of the nanotubes to ribbons. Figure 2c,d shows that unzipping of Li_xWS₂-NTs results in 1D nanostructures of increased width

(~ 100 nm) and linear edges while retaining the micrometer length. In addition to curved (nanotrough) WS_2 -NRs (Figure 2c), few flat WS_2 -NRs were also observed (Figure 2d). Low-magnification bright-field TEM images (Supporting Information, Figure S2a,b) show a large number of curved and/or kinked WS_2 -NRs. The extent of unzipping was evaluated from the TEM images of the sample on several copper grids. We could hardly see any Li_xWS_2 -NTs that remained unaffected, as 95% of the Li_xWS_2 -NTs were unzipped to yield either flat or curved WS_2 -NRs.

HRTEM images of the edges of curved WS_2 -NRs (Figure 3a,b) clearly indicate that the ribbons are multilayered (10–12 layers) with an interlayer spacing of 6.2 Å corresponding to the (002) planes of WS_2 . This suggests that the reaction of octanethiol with Li_xWS_2 -NTs causes longitudinal cutting of the tubes accompanied by little or no exfoliation. The curved nature of the multilayered ribbons could possibly be due to the residual strain between the unseparated layers. Figure 3c,d shows the HRTEM images of the edges of flat WS_2 -NRs showing the (101) in plane lattices and crystalline wavy edges. The electron diffraction pattern obtained from the same region (inset in Figure 3d) is indexed to hexagonal WS_2 .

The AFM images (Figure 4) further support the TEM observations. Figure 4a clearly reveals the longitudinal unzipping of a Li_xWS_2 -NT. The smooth incision along the length of the tube and the corresponding height profile indicate that the reaction of Li_xWS_2 with octanethiol is well-controlled and facile. A ~ 12 nm thick WS_2 -NR (Figure 4b) indicates that the multiwalled nature of the nanotubes is retained in the nanoribbons, as observed in the HRTEM images (Figure 3a,b).

Figure 5 compares the Raman spectrum of WS_2 -NRs with that of the WS_2 bulk. WS_2 -NRs exhibit bands at 419.4 and 353.7 cm^{-1} due to A_{1g} and E_{2g} modes with full width at half-maximum (fwhm) of 7.4 and 11.6 cm^{-1} , respectively. Corresponding bands in the case of bulk occur at 422.6 and 352.8 cm^{-1} with fwhm of 3.9 and 9.7 cm^{-1} . This clearly suggests softening of A_{1g} and E_{2g} modes and phonon confinement in WS_2 -NRs, as expected for few-layered nanosheets.³⁵ Electron energy loss spectrum (EELS) of WS_2 -NRs shows only characteristic W-M(4,5) and S-L(2,3) edges with no signals due to impurities (Supporting Information, Figure S3).

Composition analysis of WS_2 -NRs was carried out using high-angle annular dark-field (HAADF) scanning transmission electron microscopy (STEM) and EDS elemental mapping. Figure 6a,d presents HAADF STEM images of two different WS_2 -NRs: a curved one and a flat one. The elemental maps of the constituting elements W and S (Figure 6b,c,e,f) clearly demonstrate a well-defined compositional profile of [W/S = 1:2].

Chemical composition of the WS_2 -NRs was further examined by X-ray photoelectron spectroscopy (XPS).

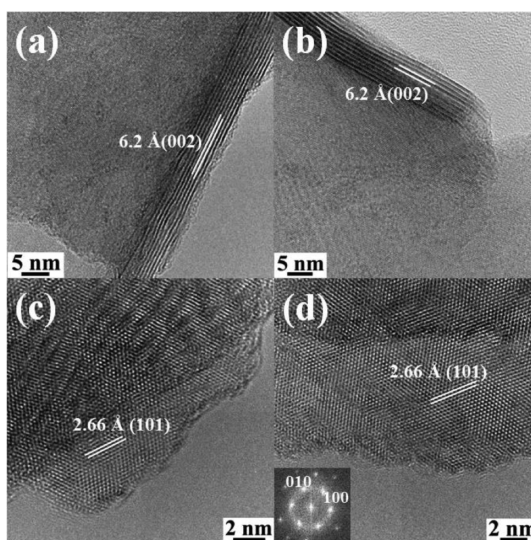


Figure 3. HRTEM images of WS_2 -NRs obtained by unzipping Li_xWS_2 -NTs using octanethiol. (a,b) Partially wrapped ribbon edges showing a 6.2 Å interlayer separation; (c,d) fully unwrapped ribbons revealing the atomically resolved basal planes with a 2.66 Å fringe separation.

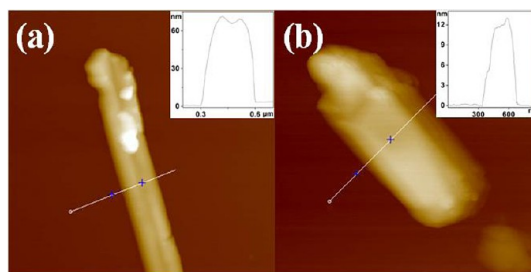


Figure 4. AFM images of WS_2 -NRs obtained by unzipping Li_xWS_2 -NTs using octanethiol. Image in (a) reveals a tube neatly unzipped along its length by octanethiol, and image in (b) is of a flat WS_2 -NR.

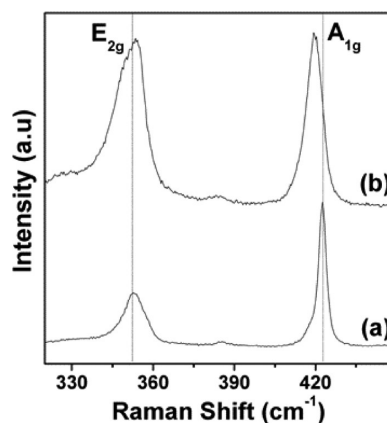


Figure 5. Comparative Raman spectra of bulk WS_2 (a) and WS_2 -NRs obtained by unzipping Li_xWS_2 -NTs using octanethiol (b).

The W4f and S2p regions of the XPS spectra for WS_2 -NRs are shown in Figure 7a,b. The W4f_{7/2} and W4f_{5/2} peaks appearing at 33.14 and 35.45 eV correspond

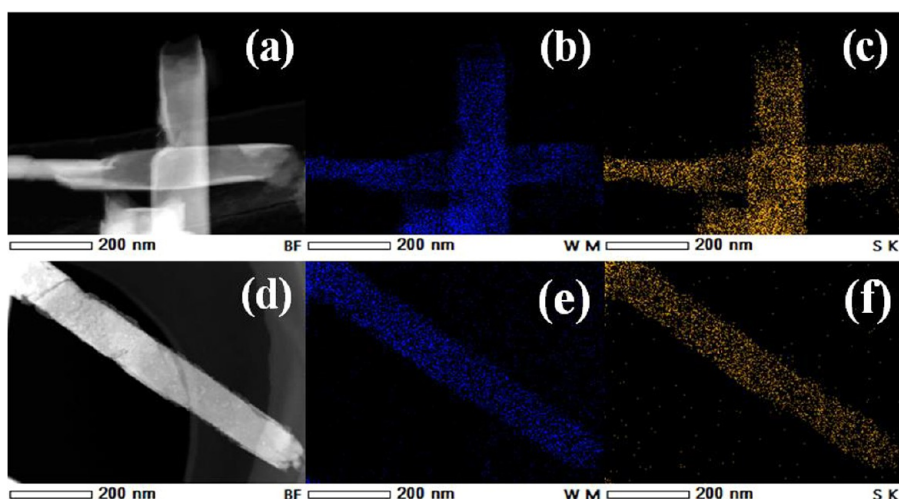


Figure 6. HAADF STEM images (a,d) and the spatially resolved W (b,e) and S (c,f) elemental maps of the WS_2 -NRs obtained by unzipping Li_xWS_2 -NTs using octanethiol.

to W^{4+} . Similarly, the $S2p_{3/2}$ and $S2p_{1/2}$ peaks appearing at 162.75 and 163.93 eV correspond to S^{2-} . These are in accordance with the 2H- WS_2 phase.³⁶ Thus, the XPS studies confirm that the WS_2 -NRs obtained by unzipping Li_xWS_2 -NTs using octanethiol are free from impurities and remain unoxidized.

In the case of the product obtained on reaction of Li_xWS_2 -NTs with water, the W4f XPS spectrum (Supporting Information, Figure S4) shows two sets of peaks. The $W4f_{7/2}$ and $W4f_{5/2}$ peaks appearing at 33.74 and 35.93 eV correspond to W^{4+} , while the intense peaks at 35.46 and 37.64 eV correspond to W^{6+} . The $S2p$ XPS spectrum (Figure S4) exhibits two doublets, the intense one at 160.48 and 161.65 eV and the other at 162.33 and 163.54 eV corresponding to 1T and 2H phases of WS_2 , respectively.³⁶ In addition, a peak at 168 eV due to SO_2 is observed in the expanded $S2p$ XPS spectrum (Supporting Information, Figure S4). These results suggest that unzipping of Li_xWS_2 -NTs in oxygen-containing solvents would result in a product that is largely oxidized. WS_2 is easily oxidized compared to MoS_2 because the heat of formation of oxide from sulfide in the case of W is 15 kcal/mol higher than that in the case of Mo.³³

Reducing the aggression of the reaction between the intercalated Li and the solvent seems to be the key for the successful unzipping of the tubes. The molecular sizes of the solvents employed in this work are as follows: water -2.8 \AA , ethanol -3.8 \AA , alkyl chain lengths of octanethiol -13.3 \AA , and dodecanethiol -15.2 \AA (the size of the headgroup of the alkanethiols is same as that of H_2S , which is 3.8 \AA). The interlayer spacing of Li_xWS_2 -NTs is 11.4 \AA and that of WS_2 nanotubes is 6.2 \AA (Supporting Information, Figure S1d). Thus the gallery height (the gap between two adjacent layers) is 5.2 \AA . Water and ethanol molecules that are much smaller than the gallery height are easily accommodated in the interlayer space accounting for

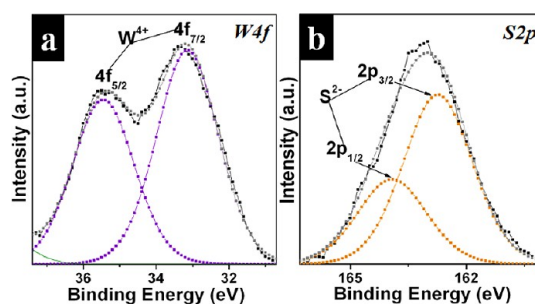
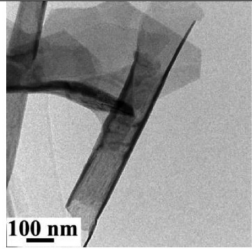
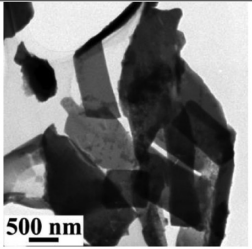


Figure 7. Core level W4f (a) and $S2p$ (b) XPS spectra of WS_2 -NRs obtained by unzipping Li_xWS_2 -NTs using octanethiol.

their faster diffusion into the interlayer. The fast diffusing water and ethanol react violently with the intercalated Li (reactions 1 and 2), causing complete/partial destruction of the tubes. In the case of larger thiol molecules, the headgroup ($-SH$) enters the interlayer gallery first and the large alkyl chain tail blocks the passage for next molecule. This causes slower diffusion of the solvent molecules into the interlayer of Li_xWS_2 -NTs and reduction of the aggression of the reaction (reaction 3) leading to controlled scissoring of the WS_2 -NTs to yield WS_2 -NRs.

In order to see if the aggression of the reaction between the intercalated Li and the solvent is indeed controlling the way in which the tubes break, the aggression of the reaction between octanethiol and Li_xWS_2 -NTs was increased by increasing the Li content in Li_xWS_2 -NTs. In Table 1, we compare the results of the reaction between Li_xWS_2 -NTs and octanethiol when $x = 0.9$ and 1.2 . While $Li_{0.9}WS_2$ -NTs obtained by lithiation at $80 \text{ }^\circ\text{C}$ were neatly unzipped on reaction with octanethiol, $Li_{1.2}WS_2$ -NTs obtained by lithiation at $100 \text{ }^\circ\text{C}$ reacted more vigorously with octanethiol to give largely broken pieces with a few unzipped structures. This further confirms that the reaction needs to be less aggressive for the successful unzipping of these reactive tubes.

TABLE 1. Summary of the Effect of Lithiation Temperature on Unzipping of Li_xWS_2 -NTs

Temperature ($^{\circ}\text{C}$)	80	100
Mole fraction (x) of Li in Li_xWS_2 -NTs	0.91 ± 0.05	1.18 ± 0.06
Product obtained in the reaction between Li_xWS_2 -NTs and octanethiol		

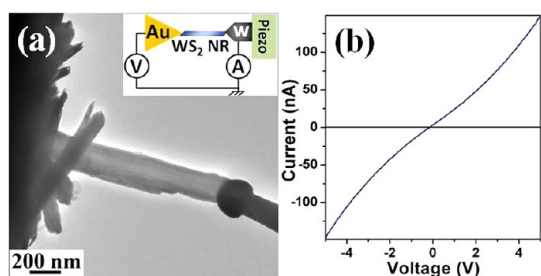


Figure 8. (a) TEM image of a ribbon connected to the counter gold electrode and tungsten STM tip. The inset represents the experimental configuration. (b) I - V curve of a WS_2 -NR obtained by unzipping Li_xWS_2 -NTs using octanethiol.

The probable mechanism of the tube unzipping could be as follows. Initially, the octanethiol molecules enter into the interlayer region of Li_xWS_2 -NTs through some defect sites on the surface of the tubes and/or through the open ends of the tubes, causing an increase in the stress at the site of entry. This leads to breaking of W-S bonds in the stressed regions. This initial incision becomes the target for more octanethiol molecules to enter and the building up of stress and incision progress longitudinally. More details on the unzipping mechanism, as revealed by molecular dynamic simulations, will be separately reported elsewhere.

The electrical properties of WS_2 -NRs were measured using a "Nanofactory Instruments" scanning tunneling

microscopy (STM)-TEM holder integrated in the HRTEM.^{37,38} As illustrated in Figure 8a, a WS_2 -NR initially attached to a gold counter electrode is brought in contact with the STM tungsten tip, and subsequently, current was measured at various potentials. Preliminary electrical measurements indicate that the representative I - V curve is characteristic of an Ohmic behavior, suggesting that the WS_2 -NR is a conductor with resistance of 40 M Ω . Theoretical studies have suggested that metallic WS_2 -NRs should have zigzag edges.¹³ A detailed systematic investigation on electrical transport of WS_2 -NRs could possibly give insights into the relation between their electrical properties and the width and nature of WS_2 ribbon edges.

CONCLUSION

Near quantitative unzipping of multiwalled WS_2 nanotubes has been achieved through Li intercalation followed by the reaction of the intercalated Li and long chain thiols. The extent of unzipping observed here is far higher than the same observed in carbon nanotubes (CNTs) and boron nitride nanotubes (BNNTs). The use of thiol solvents prevents formation of oxide impurities. The fact that the bonding in WS_2 is much weaker than that in CNT/BNNT and the chalcogenide system is chemically more fragile make the unzipping of WS_2 nanotubes quite significant.

METHODS

Lithiation of WS_2 Nanotubes (Li_xWS_2 -NTs). Dry multiwalled WS_2 nanotubes (500 mg, 2 mmol) purchased from NanoMaterials Ltd. (Israel) were added to 20 mL of 0.17 M solution of *n*-butyllithium (BuLi) in hexane, and the mixture was sealed in a Teflon-lined autoclave (60 mL capacity). The autoclave was heated at 80 $^{\circ}\text{C}$ for 24 h and slowly cooled to room temperature. The black product obtained was washed repeatedly with dry *n*-hexane to remove unreacted BuLi and other soluble impurities and stored under *n*-hexane. Hereafter, this sample is referred to as Li_xWS_2 -NTs. The lithiation of WS_2 tubes was also carried out at 100 $^{\circ}\text{C}$ to study the effect of the Li content in Li_xWS_2 -NTs on the unzipping reaction.

Unzipping of Li_xWS_2 -NTs. About 100 mg of Li_xWS_2 -NTs was transferred to a beaker containing 10 mL of the desired solvent. The reactions were carried out using various solvents such as water, methanol, ethanol, octanethiol, and dodecanethiol. The Li_xWS_2 -NTs were allowed to react with solvent without agitation, or they were sonicated for 1 min in the solvent in separate experiments. In all the cases, stable colloidal dispersions were obtained. The solid products were coagulated from the dispersions by the addition of acetone. The coagulated solids were filtered and dried under vacuum. In the case of reaction with thiols, the products were washed repeatedly with small amounts of ethanol-water mixture to remove lithium salts.

Estimation of Lithium Content in $\text{Li}_x\text{WS}_2\text{-NTs}$. The Li content in $\text{Li}_x\text{WS}_2\text{-NTs}$ obtained under different reaction conditions was estimated by ion chromatography using a Metrohm 861 advanced compact ion chromatograph with Metrosep C 250 cation column and conductivity detector. About 100 mg of $\text{Li}_x\text{WS}_2\text{-NTs}$ was mixed with 25 mL of water to get a colloidal dispersion. Twenty-five milliliters of acetone was added to the dispersion to coagulate the solid. The supernatant was collected by decantation. The solid was redispersed in water and coagulated again by adding acetone. The supernatant was collected as before, and this cycle was repeated six times. The collected supernatant was evaporated to dryness, the solid residue was dissolved in water, and the solution was suitably diluted for ion chromatographic analysis.

Characterization. All the samples were analyzed by recording powder X-ray diffraction (XRD) patterns using a PANalytical X'pert pro diffractometer (Cu $K\alpha$ radiation, secondary graphite monochromator, at a scanning rate of 2° $2\theta/\text{min}$). Scanning electron microscopy (SEM) images were recorded on a Hitachi S4800 electron microscope operating at 15 kV. Transmission electron microscopy (TEM) images were taken with a JEOL-3000F microscope operated at 300 kV. Atomic force microscopy (AFM) images were acquired with a diNanoscope (digital instruments/Veeco) operating in tapping mode, using a Si tip cantilever with a force constant of 20 N m^{-1} . Sample for AFM analysis was prepared by spin coating an ethanolic dispersion of WS_2 nanoribbons at 3000 rpm onto a Si substrate. X-ray photoelectron spectroscopy measurements were carried out with an ESCA-Lab220i-XL spectrometer using a twin-anode Al $K\alpha$ (1486.6 eV) X-ray source. All spectra were calibrated to the binding energy of the C1s peak at 284.51 eV. The base pressure was around 3×10^{-7} Pa. Raman spectra were recorded on a Horiba Jobin-Yvon T6400 Raman spectrometer using a 632 nm HeNe laser.

Conflict of Interest: The authors declare no competing financial interest.

Acknowledgment. The authors thank Drs. Yamada, K. Iiyama, A. Nukui, and M. Mitome for their generous technical assistance. This work was funded by the World Premier International Center for Materials Nanoarchitectonics (WPI-MANA) of NIMS, Tsukuba, Japan. A.J. and M.R. acknowledge funding of this work by DST, India (SR/S1/PC-23/2011). R.T. acknowledges the support of the EU-ITN project MoWSeS (317451).

Supporting Information Available: SEM and TEM images, XRD, EELS and XPS analysis of $\text{WS}_2\text{-NRs}$. This material is available free of charge via the Internet at <http://pubs.acs.org>.

REFERENCES AND NOTES

- James, D. K.; Tour, J. M. The Chemical Synthesis of Graphene Nanoribbons—A Tutorial Review. *Macromol. Chem. Phys.* **2012**, *213*, 1033–1050.
- Ma, L.; Wang, J.; Ding, F. Recent Progress and Challenges in Graphene Nanoribbon Synthesis. *ChemPhysChem.* **2013**, *14*, 47–54.
- Nakada, K.; Fujita, M.; Dresselhaus, G.; Dresselhaus, M. S. Edge State in Graphene Ribbons: Nanometer Size Effect and Edge Shape Dependence. *Phys. Rev. B* **1996**, *54*, 17954–17961.
- Son, Y.-W.; Cohen, M. L.; Louie, S. G. Energy Gaps in Graphene Nanoribbons. *Phys. Rev. Lett.* **2006**, *97*, 216803(1)–216807(4).
- Park, C.-H.; Louie, S. G. Energy Gaps and Stark Effect in Boron Nitride Nanoribbons. *Nano Lett.* **2008**, *8*, 2200–2203.
- Barone, V.; Peralta, J. E. Magnetic Boron Nitride Nanoribbons with Tunable Electronic Properties. *Nano Lett.* **2008**, *8*, 2210–2214.
- Wells, A. F. *Structural Inorganic Chemistry*, 4th ed.; The English Language Book Society and Oxford University Press: London, 1979.
- Alberti, G.; Costantino, U. Two and Three Dimensional Inorganic Networks. In *Comprehensive Supramolecular Chemistry*; Alberti, G., Bein, T., Eds.; Pergamon: New York, 1977; Vol. 7.
- Novoselov, K. S.; Jiang, D.; Schedin, F.; Booth, T. J.; Khotkevich, V. V.; Morozov, S. V.; Geim, A. K. Two-Dimensional Atomic Crystals. *Proc. Natl. Acad. Sci. U.S.A.* **2005**, *102*, 10451–10453.
- Li, Y.; Zhou, Z.; Zhang, S.; Chen, Z. MoS_2 Nanoribbons: High Stability and Unusual Electronic and Magnetic Properties. *J. Am. Chem. Soc.* **2008**, *130*, 16739–16744.
- Wang, Z.; Li, H.; Liu, Z.; Shi, Z.; Lu, J.; Suenaga, K.; Joung, S.-K.; Okazaki, T.; Gu, Z.; Zhou, J.; et al. Mixed Low-Dimensional Nanomaterial: 2D Ultranarrow MoS_2 Inorganic Nanoribbons Encapsulated in Quasi-1D Carbon Nanotubes. *J. Am. Chem. Soc.* **2010**, *132*, 13840–13847.
- Botello-Méndez, A. R.; López-Urías, F.; Terrones, M.; Terrones, H. Metallic and Ferromagnetic Edges in Molybdenum Disulfide Nanoribbons. *Nanotechnology* **2009**, *20*, 325703–325709.
- Wang, Z.; Zhao, K.; Li, H.; Liu, Z.; Shi, Z.; Lu, J.; Suenaga, K.; Joung, S.-K.; Okazaki, T.; Jin, Z.; et al. Ultra-Narrow WS_2 Nanoribbons Encapsulated in Carbon Nanotubes. *J. Mater. Chem.* **2011**, *21*, 171–180.
- Remikar, M.; Skraba, Z.; Regula, M.; Ballif, C.; Sanjines, R.; Levy, F. New Crystal Structures of WS_2 : Microtubes, Ribbons, and Ropes. *Adv. Mater.* **1998**, *10*, 246–249.
- Li, X.; Wang, X.; Zhang, L.; Lee, S.; Dai, H. Chemically Derived, Ultrasoft Graphene Nanoribbon Semiconductors. *Science* **2008**, *319*, 1229–1232.
- Chen, L.; Hernandez, Y.; Feng, X.; Mullen, K. From Nanographene and Graphene Nanoribbons to Graphene Sheets: Chemical Synthesis. *Angew. Chem., Int. Ed.* **2012**, *51*, 7640–7654.
- Jiao, L.; Zhang, L.; Wang, X.; Diankov, G.; Dai, H. Narrow Graphene Nanoribbons from Carbon Nanotubes. *Nature* **2009**, *458*, 877–880.
- Zeng, H.; Zhi, C.; Zhang, Z.; Wei, X.; Wang, X.; Guo, W.; Bando, Y.; Golberg, D. “White Graphenes”: Boron Nitride Nanoribbons via Boron Nitride Nanotube Unwrapping. *Nano Lett.* **2010**, *10*, 5049–5055.
- Kosynkin, D. V.; Higginbotham, A. L.; Sinitskii, A.; Lomeda, J. R.; Dimiev, A.; Price, B. K.; Tour, J. M. Longitudinal Unzipping of Carbon Nanotubes to Form Graphene Nanoribbons. *Nature* **2009**, *458*, 872–876.
- Cataldo, F.; Compagnini, G.; Patane, G.; Ursini, O.; Angelini, G.; Ribic, P. R.; Margaritondo, G.; Cricenti, A.; Palleschi, G.; Valentini, F. Graphene Nanoribbons Produced by the Oxidative Unzipping of Single-Wall Carbon Nanotubes. *Carbon* **2010**, *48*, 2596–2602.
- Cano-Marquez, A. G.; Rodriguez-Macias, F. J.; Campos-Delgado, J.; Espinosa-Gonzalez, C. G.; Tristan-Lopez, F.; Ramirez-Gonzalez, D.; Cullen, D. A.; Smith, D. J.; Terrones, M.; Vega-Cantu, Y. I. Ex-MWNTs: Graphene Sheets and Ribbons Produced by Lithium Intercalation and Exfoliation of Carbon Nanotubes. *Nano Lett.* **2009**, *9*, 1527–1533.
- Kosynkin, D. V.; Lu, W.; Sinitskii, A.; Pera, G.; Sun, Z.; Tour, J. M. Highly Conductive Graphene Nanoribbons by Longitudinal Splitting of Carbon Nanotubes Using Potassium Vapor. *ACS Nano* **2011**, *5*, 968–974.
- Erickson, K. J.; Gibb, A. L.; Sinitskii, A.; Rouseas, M.; Alem, N.; Tour, J. M.; Zettl, A. K. Longitudinal Splitting of Boron Nitride Nanotubes for the Facile Synthesis of High Quality Boron Nitride Nanoribbons. *Nano Lett.* **2011**, *11*, 3221–3226.
- Elias, A. L.; Botello-Mendez, A. R.; Meneses-Rodriguez, D.; Gonzalez, V. J.; Ramirez-Gonzalez, D.; Ci, L.; Munoz-Sandoval, E.; Ajayan, P. M.; Terrones, H.; Terrones, M. Longitudinal Cutting of Pure and Doped Carbon Nanotubes to Form Graphitic Nanoribbons Using Metal Clusters as Nanoscalpels. *Nano Lett.* **2010**, *10*, 366–372.
- Parashar, U. K.; Bhandari, S.; Srivastava, R. K.; Jariwala, D.; Srivastava, A. Single Step Synthesis of Graphene Nanoribbons by Catalyst Particle Size Dependent Cutting of Multi-walled Carbon Nanotubes. *Nanoscale* **2011**, *3*, 3876–3882.
- Shinde, D. B.; Debgupta, J.; Kushwaha, A.; Aslam, M.; Pillai, V. K. Electrochemical Unzipping of Multi-Walled Carbon Nanotubes for Facile Synthesis of High-Quality Graphene Nanoribbons. *J. Am. Chem. Soc.* **2011**, *133*, 4168–4171.

27. Jiao, L.; Wang, X.; Diankov, G.; Wang, H.; Dai, H. Facile Synthesis of High-Quality Graphene Nanoribbons. *Nat. Nanotechnol.* **2010**, *5*, 321–325.
28. Xie, L.; Wang, H.; Jin, C.; Wang, X.; Jiao, L.; Suenaga, K.; Dai, H. Graphene Nanoribbons from Unzipped Carbon Nanotubes: Atomic Structures, Raman Spectroscopy, and Electrical Properties. *J. Am. Chem. Soc.* **2011**, *133*, 10394–10397.
29. Kumar, P.; Panchakarla, L. S.; Rao, C. N. R. Laser-Induced Unzipping of Carbon Nanotubes to Yield Graphene Nanoribbons. *Nanoscale* **2011**, *3*, 2127–2129.
30. Tenne, R.; Margulis, L.; Genut, M.; Hodes, G. Polyhedral and Cylindrical Structures of Tungsten Disulphide. *Nature* **1992**, *360*, 444–446.
31. Tenne, R. Inorganic Nanotubes and Fullerene-like Nanoparticles. *Nat. Nanotechnol.* **2006**, *1*, 103–111.
32. Bar-Sadan, M.; Houben, L.; Enyashin, A. N.; Seifert, G.; Tenne, R. Atom by Atom: HRTEM Insights into Inorganic Nanotubes and Fullerene-like Structures. *Proc. Natl. Acad. Sci. U.S.A.* **2008**, *105*, 15643–15648.
33. Miremedi, B. K.; Morrison, S. R. The Intercalation and Exfoliation of Tungsten Disulfide. *J. Appl. Phys.* **1988**, *63*, 4970–4974.
34. Yang, D.; Frindt, R. F. Li-Intercalation and Exfoliation of WS_2 . *J. Phys. Chem. Solids* **1996**, *57*, 1113–1116.
35. Frey, G. L.; Tenne, R.; Matthews, M. J.; Dresselhaus, M. S.; Dresselhaus, G. Raman and Resonance Raman Investigation of MoS_2 Nanoparticles. *Phys. Rev. B* **1999**, *60*, 2883–2892.
36. Eda, G.; Yamaguchi, H.; Voiry, D.; Fujita, T.; Chen, M.; Chhowalla, M. Photoluminescence from Chemically Exfoliated MoS_2 . *Nano Lett.* **2011**, *11*, 5111–5116.
37. Bai, X.; Golberg, D.; Bando, Y.; Zhi, C.; Tang, C.; Mitome, M.; Kurashima, K. Deformation-Driven Electrical Transport of Individual Boron Nitride Nanotubes. *Nano Lett.* **2007**, *7*, 632–637.
38. Tang, D. M.; Yin, L. C.; Li, F.; Liu, C.; Yu, W. J.; Hou, P. X.; Wu, B.; Lee, Y. H.; Ma, X. L.; Cheng, H. M. Carbon Nanotube-Clamped Metal Atomic Chain. *Proc. Natl. Acad. Sci. U.S.A.* **2010**, *107*, 9055–9059.